Modeling elastic instabilities in nematic elastomers

Badel L. Mbanga,* Fangfu Ye,† Jonathan V. Selinger, and Robin L. B. Selinger‡
Liquid Crystal Institute, Kent State University, Kent, Ohio 44242, USA

(Received 17 December 2009; revised manuscript received 25 July 2010; published 1 November 2010)

Liquid crystal elastomers are cross-linked polymer networks covalently bonded with liquid crystal mesogens. In the nematic phase, due to strong coupling between mechanical strain and orientational order, these materials display strain-induced instabilities associated with formation and evolution of orientational domains. Using a three-dimensional finite element elastodynamics simulation, we investigate one such instability, the onset of stripe formation in a monodomain film stretched along an axis perpendicular to the nematic director. In our simulation, we observe the formation of striped domains with alternating director rotation. This model allows us to explore the fundamental physics governing dynamic mechanical response of nematic elastomers and also provides a potentially useful computational tool for engineering device applications.

DOI: 10.1103/PhysRevE.82.051701 PACS number(s): 61.30.Vx, 62.20.D−, 64.70.mf, 81.40.Jj

Liquid crystal elastomers (LCE) exhibit some of the elastic properties of rubber along with the orientational order properties of liquid crystals, displaying a variety of nematic and smectic phases. They are composed of liquid crystal mesogens covalently bonded to a cross-linked polymer backbone [1,2]. These materials display strong coupling between orientational order of the mesogens and mechanical deformation of the polymer network. For instance in a nematic LCE, any change in the magnitude of the nematic order parameter induces shape change, e.g., the isotropic-nematic phase transition induces strains of up to several hundred percent [3].

Conversely, applied strain can also drive changes in orientational order, producing the fascinating phenomenon of semisoft elasticity [4]. In a classic experiment, Kundler and Finkelmann [5] measured the mechanical response of a monodomain nematic LCE thin film stretched along an axis perpendicular to the nematic director. They observed a semisoft elastic response with a pronounced plateau in the stress-strain curve arising at a threshold stress. Accompanying this instability they observed the formation of striped orientational domains with alternating sense of director rotation, and a stripe width of 15 μm. They repeated the experiment with samples cut at different orientations to the director axis, and found that the instability was absent when the angle between the initial director and the stretch axis was less than 70°; in this geometry, instead of forming stripes, the director rotates smoothly as a single domain.

DeSimone *et al.* [6] carried out numerical simulation studies of the stripe instability using a two-dimensional finite element elastostatic method. Each area element in the system was considered as a composite of domains with different orientations. This simulation model was the first to reproduce successfully the soft elastic response of nematic elastomers, but did not attempt to resolve the resulting microstructural evolution. Uchida [7] carried out more detailed studies of director evolution in nematic elastomers using a two-dimensional lattice model where macroscopic strain is treated as a global variable analogous to an external field, but did not attempt to describe the nonuniform strain and resulting shape evolution of the sample.

Here we explore this elastic instability in more detail by simultaneously modeling the sample's mechanical response, shape evolution, and the associated microstructural evolution as a function of strain. We use a Hamiltonian-based three-dimensional (3D) finite element elastodynamics model with terms that explicitly couple strain and nematic order. By resolving the finite element mesh down to the micron scale, we resolve the formation of orientational domains, and because the model is dynamic rather than static in character, we can examine the effects of strain rate. We use the simulation to explore the dependence of mechanical response on deformation geometry.

We model this instability in a thin film of nematic elastomer which has been cross-linked in the nematic phase. Using public domain meshing software [8] we discretize the volume of the sample into approximately 78 000 tetrahedral elements. For each volume element we assign a local variable $\mathbf{n}$ which defines the nematic director, and $Q_{ij} = \frac{1}{2}S(3n_i n_j - \delta_{ij})$ which is the associated symmetric and traceless nematic order tensor. The initial state is taken to be a monodomain with $\mathbf{n}=\mathbf{n_0}$ in every element; this configuration is defined as the system's stress-free reference state. Thus the nematic order tensor in the reference configuration Q^r_{ij} is calculated using this definition of $\mathbf{n_0}$.

There are many approaches to finite element simulation of the dynamics of elastic media [9]; we make use of an elegant Hamiltonian approach developed by Broughton *et al.* [10,11], generalizing it to three dimensions and the case of large rotations. We write the Hamiltonian of an isotropic elastic solid as

$$H_{elastic} = \sum_p V_p \frac{1}{2} C_{ijkl} \varepsilon^p_{ij} \varepsilon^p_{kl} + \sum_i \frac{1}{2} m_i v_i^2. \quad (1)$$

Here the first term represents elastic strain energy, with p summing over volume elements. V_p is the volume of element p in the reference state. For an isotropic material the components of the elastic stiffness tensor C_{ijkl} are determined from only two material parameters, namely, the shear and bulk moduli [12]. As an approximation, Broughton *et al.* devel-

*Present address: Department of Polymer Sciences and Engineering, University of Massachusetts at Amherst, Amherst, MA 01003.
†Present address: Department of Physics, University of Illinois at Urbana-Champaign, Urbana, IL 61801.
‡rselinge@kent.edu

 ©2010 The American Physical Society

oped this formulation using the linear strain tensor, but we instead use the rotationally invariant Green-Lagrange strain tensor $\varepsilon_{ij}=\frac{1}{2}(u_{i,j}+u_{j,i}+u_{k,i}u_{k,j})$, where $\mathbf{u}$ is the displacement field. We note that using the linearized strain tensor would make the Hamiltonian unphysical, as rotation of the sample would appear to cost energy. The second term represents kinetic energy in the lumped mass approximation [11] whereby the mass of each element is equally distributed among its vertices, which are the nodes of the mesh. Here i sums over all nodes, m_i is the effective mass and v_i the velocity of node i.

To account for the additional energy cost associated with the presence of a director field, we add to the potential energy,

$$H_{nematic} = \sum_p V_p[-\alpha\varepsilon_{ij}^p(Q_{ij}^p - Q_{ij}^{rp}) + \beta(Q_{ij}^p - Q_{ij}^{rp})^2] + \gamma\sum_{\langle p,q\rangle}(Q_{ij}^p - Q_{ij}^q)^2. \quad (2)$$

The first term describes coupling between the strain and order parameter tensors using a form proposed by de Gennes [13]. Here Q_{ij} defines the nematic order after deformation while Q_{ij}^r defines the preferred nematic order frozen in at cross-linking. Variables Q_{ij}, Q_{ij}^r, and ϵ_{ij} are all defined in the body frame, i.e., they are invariant under rotations in the target space [14]. The prefactor α controls the strength of this coupling, and de Gennes [13] argued that it is of the same order of magnitude as the shear modulus μ. The second term describes "cross-link memory," that is, the tendency of the nematic director to prefer its orientation at cross-linking. Thus there is an energy cost to rotate the director away from its reference state, with coupling strength β. The third term is an energy penalty for spatial variations of the nematic director, similar to a Frank free energy in the single elastic constant approximation. The summation is carried only over nearest neighbor elements in the mesh, as the typical domain size is of the order of the nematic correlation length [15].

The strain tensor ε_{ij} within each tetrahedral element is calculated in two steps. We calculate the displacement $\mathbf{u}$ of each node from the reference state, then perform a linear interpolation of the displacement field within the volume element in the reference state. The resulting interpolation coefficients represent the derivatives $u_{i,j}$ needed to calculate the components of the strain tensor. Details can be found in any introductory text on finite element methods, e.g., [16]. At this level of approximation, the strain is piecewise constant within each volume element. The effective force on each node is calculated as the negative derivative of the potential energy with respect to node displacement.

To evolve the system forward in time, we assume the director is in quasistatic equilibrium with the strain; that is, the time scale for director relaxation is much faster than that for strain evolution as observed by Urayama [17]. The first part of each step is elastodynamics: holding Q_{ij} in each element constant, the equations of motion $f=ma$ for all node positions and velocities are integrated forward in time using the Velocity Verlet algorithm [18], with a time step of 10^{-8} s. In the second part of each step, we relax the nematic director in each element to instantaneously minimize the element's potential energy. Because the director relaxes from a higher energy state to a lower energy state without picking up conjugate momentum, this is a source of anisotropic dissipation. Thus in our model, as in real nematic elastomers, strains that rotate the director cause more energy dissipation than those applied parallel to the director [19].

To add internal damping associated with velocity gradients in the sample, we use a modified form of Kelvin dissipation. In its standard form, the Kelvin dissipation force (e.g., between two particles, or between two nodes in a finite element mesh) is proportional to the velocity difference between them (see, e.g., [20].) This form conserves linear momentum but violates conservation of angular momentum; internal dissipation forces could create torque, which is of course unphysical. We modified the Kelvin dissipation form to provide for conservation of angular momentum, that is, dissipation forces between any pair of nodes must act along the line of sight between them, so they create no torque [21]. We also scale the dissipation force so it depends on the effective strain rate between two nodes rather than their absolute velocity difference. With these modifications, the dissipation force between a pair of neighboring nodes separated by distance d is $\mathbf{F}_{12}=-\eta(\mathbf{v}_1-\mathbf{v}_2)\cdot(\mathbf{r}_1-\mathbf{r}_2)\hat{r}_{12}/d$, with $\eta=10^{-5}$ kg/s. $\hat{r}_{12}$ is a unit vector along the line of sight between the nodes. The resulting dissipation is isotropic in character and does not depend on the orientation of the director field.

We simulate uniaxial stretching in an initially monodomain nematic elastomer film of size 1.5 mm $\times$ 0.5 mm with a thickness of 50 μm, with shear modulus $\mu=5.7\times10^5$ Pa, bulk modulus $B_r=2.8\times10^7$ Pa, and parameters $\alpha=\mu$, $\beta=0.3\mu$, and $\gamma=10^{-7}$ J. For convenience, the scalar order parameter S is set to be 1. We first consider the case where the director is initially oriented along the y axis, transverse to the direction of applied strain. The sample is clamped on two sides and the clamped regions are constrained to move apart laterally at a constant speed of 1 mm/s. The resulting microstructural evolution is shown in Fig. 1. Here, color represents Jones matrix imaging of the director field as viewed through crossed polarizers parallel to the x and y directions; blue corresponds to a director parallel to the polarizer or analyzer, and red corresponds to a director at a 45° angle to either. While the simulated sample is three-dimensional, the film's microstructure does not vary significantly through the thickness and can thus be visualized in two dimensions (2D).

At a strain of 8.5%, the director field in the sample becomes unstable and orientational domains form, nucleating first from the free edges of the film. Heterogeneity in the finite element mesh serves to break the symmetry and nucleate the instability. By 9% strain, the whole film is occupied by striped orientational domains with alternating sense of director rotation. The stripes are not uniform in width, being slightly larger near the free edges. Near the center of the sample, each individual stripe has a width of about 25 μm, which is of the same order of magnitude as that observed in experiment [5]. This value is in reasonable agreement with the theoretical estimate by Warner and Terentjev [1] who predicted a stripe width of $h\sim\sqrt{\xi L}/\sqrt{1-1/\lambda_1^3}$; where ξ is the

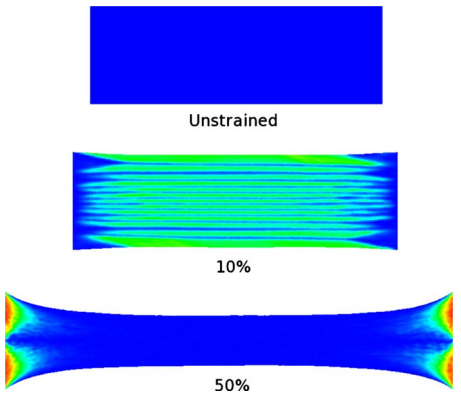

FIG. 1. (Color online) Simulation: stretching a nematic elastomer film at an angle of 90° to the director. Initially a monodomain, the director field evolves to form a striped microstructure. Darkest regions have director parallel or perpendicular to the stretching direction; brightest regions have director oriented at ±45° to the stretching direction.

nematic penetration length, L is the sample width, and λ_1 is the strain threshold of the instability. The stripes coarsen as the elongation increases. Eventually this microstructure evolves into a more disordered state with stripes at multiple orientations. By reaching 35% strain, the stripes have vanished and the film is again in a monodomain state with the director oriented with the direction of strain. Only the regions near the clamped edges do not fully realign, in agreement with experimental observations [5] and with the simulation studies of DeSimone [6]. We will explore the dependence of stripe width on aspect ratio and other parameters in future work.

The resulting stress-strain response is semisoft [14] in character, as shown in Fig. 2. The initial elastic response is linear, followed by an extended plateau running from about 8.5% to over 30% strain, after which there is a second linear regime. We also measure the average director rotation $\langle \sin^2(\phi) \rangle$ and observe that the thresholds for both the stress-strain plateau and the rotation of the nematic director occur

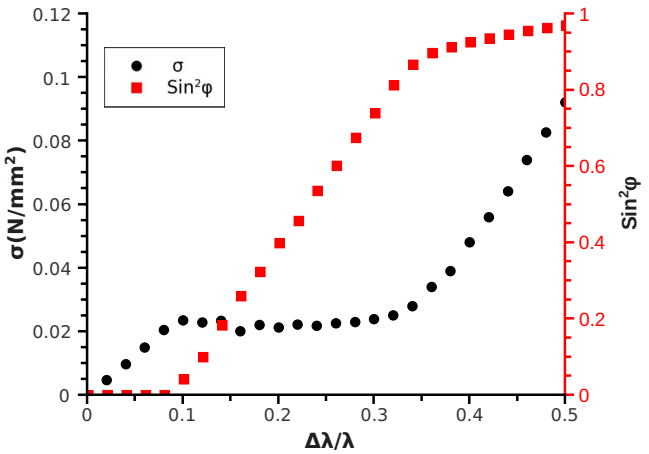

FIG. 2. (Color online) Engineering stress (circles) and director rotation (squares) vs applied strain, for the system shown in Fig. 1. Onset of director rotation and the stress-strain plateau both occur at the same strain.

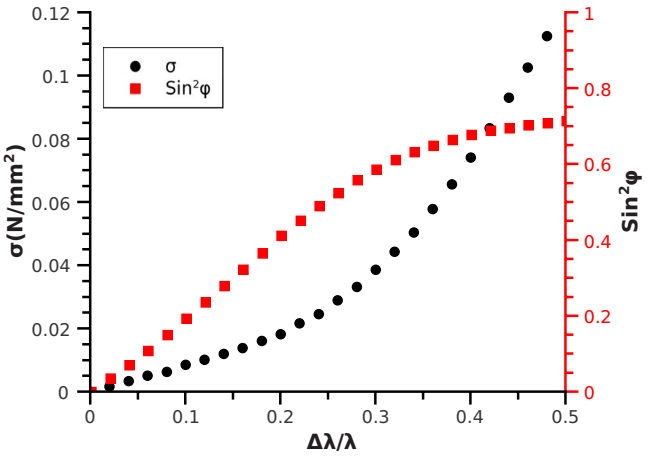

FIG. 3. (Color online) Engineering stress (circles) and director rotation (squares) vs applied strain, applied at an angle of 60° from the nematic director.

at the same strain. This finding demonstrates, in agreement with theory [1,14], that the reorientation of the system's internal degree of freedom—namely, the nematic director—reduces the energy cost of the deformation.

We also performed simulations for monodomain nematic elastomer films with the initial director orientation at different angles to the pulling direction. In Fig. 3, we plot the film's stress-strain response when strain is applied at an angle of 60° from the nematic director, which shows no plateau, and likewise director rotation shows no threshold behavior. As shown in Fig. 4, the director rotates to align with the strain direction without forming stripes. We performed additional simulations with the director at angles of 70° and 80° to the pulling direction and again found no stripe formation and no plateau in the stress-strain response.

We also tried varying the applied strain rate. Figure 5 compares the stress-strain response for samples strained at 1 and 5 mm/s. The higher strain rate produces a significant stress overshoot, and stripe formation occurs at a strain of

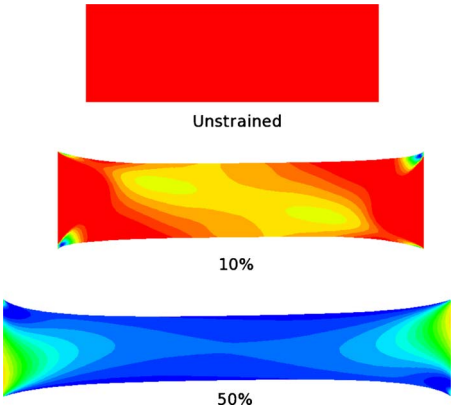

FIG. 4. (Color online) Simulation: stretching a nematic elastomer film at an angle of 60° to the director. Initially a monodomain, the director field rotates smoothly without sharp gradients in orientation. Darkest regions have director parallel or perpendicular to the stretching direction; brightest regions have director oriented at ±45° to the stretching direction.

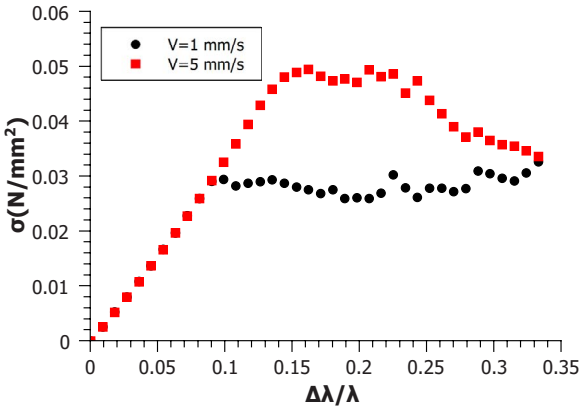

FIG. 5. (Color online) Dependence of the stress-strain response on strain rate.

15%. This finding suggests that the threshold strain for the instability depends in a significant way on strain rate.

To explore mechanical response of nematic elastomer films in a more complex geometry, we next simulated the radial stretching of a circular monodomain film of diameter 1 cm and thickness 100 μm, with the nematic director oriented initially along the y axis, as indicated by the arrow in Fig. 6. Boundary conditions were imposed that clamp the sample around its circumference and stretch radially in all directions, pulling the edge outward at constant speed. Figure 6 shows the film at different stages of its extension, demonstrating that the director field smoothly changes from a monodomain to a radial configuration, with no stripe instability. With a careful choice of the sample's thickness, this deformed circular sheet of nematic elastomer could be used as a tunable spatial polarization converter as described in [22].

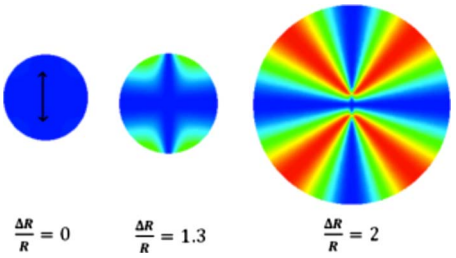

FIG. 6. (Color online) Simulation: A nematic elastomer disk is stretched radially. The director field smoothly transforms from a homogeneous vertically oriented monodomain to a nearly radial configuration.

The simulations presented here were performed at far higher strain rates, e.g., 50% per second, than those used in typical experiments [5,23] where the material is allowed to relax for minutes or hours between strain increments. In future work we plan to apply our model to examine deformation of nematic elastomers at slower strain rates and as a function of sample geometry. We will also examine the role of initial microstructure and thermomechanical history in determining mechanical response. Using the same finite element approach, we can also test the predictions of other proposed constitutive models, and model geometries of interest for potential applications. Through this approach we hope to bridge the divide between fundamental theory of these fascinating materials and engineering design of devices.

We thank T. Lubensky, M. Warner, E. Terentjev, and A. DeSimone for fruitful discussions. This work was supported by NSF Grant No. DMR-0605889, daytaOhio, and the Ohio Supercomputer Center. F.Y. also acknowledges the Institute for Complex Adaptive Matter—Branches Cost Sharing Fund for support.

[1] M. Warner and E. Terentjev, *Liquid Crystal Elastomers* (Oxford Science, Oxford, 2003).
[2] H. P. H. R. Brand and P. Martinoty, Soft Matter **2**, 182 (2006).
[3] J. Naciri, A. Srinivasan, H. Jeon, N. Nikolov, P. Keller, and B. R. Ratna, Macromolecules **36**, 8499 (2003); S. M. Clarke, A. Hotta, A. R. Tajbakhsh, and E. M. Terentjev, Phys. Rev. E **64**, 061702 (2001).
[4] F. Ye, R. Mukhopadhyay, O. Stenull, and T. C. Lubensky, Phys. Rev. Lett. **98**, 147801 (2007).
[5] I. Kundler and H. Finkelmann, Macromol. Rapid Commun. **16**, 679 (1995).
[6] S. Conti, A. DeSimone, and G. Dolzmann, Phys. Rev. E **66**, 061710 (2002).
[7] N. Uchida, Phys. Rev. E **60**, R13 (1999).
[8] Documentation and software available at http://www.salome-platform.org/
[9] T. Belytschko, W. K. Liu, and B. Moran, *Nonlinear Finite Elements for Continua and Structures* (Wiley, New York, 2000).
[10] J. Q. Broughton, F. F. Abraham, N. Bernstein, and E. Kaxiras, Phys. Rev. B **60**, 2391 (1999).
[11] R. E. Rudd and J. Q. Broughton, Phys. Rev. B **58**, R5893 (1998).
[12] M. P. Marder, *Condensed Matter Physics* (Wiley, New York, 2000).
[13] P. G. de Gennes, C. R. Seances Acad. Sci., Ser. B **281**, 101 (1975).
[14] O. Stenull and T. C. Lubensky, Phys. Rev. E **74**, 051709 (2006).
[15] S. V. Fridrikh and E. M. Terentjev, Phys. Rev. E **60**, 1847 (1999).
[16] W. B. Zimmerman, *Process Modelling and Simulation with Finite Element Methods* (World Scientific, Singapore, 2004).
[17] K. Urayama, S. Honda, and T. Takigawa, Phys. Rev. E **74**, 041709 (2006).
[18] M. Allen and D. Tildesley, *Computer Simulations of Liquids* (Clarendon, Oxford, 1987).
[19] E. M. Terentjev, I. V. Kamotski, D. D. Zakharov, and L. J. Fradkin, Phys. Rev. E **66**, 052701 (2002).
[20] M. Marder, J. Mech. Phys. Solids **54**, 491 (2006).
[21] E. L. Wilson, *Three Dimensional Static and Dynamic Analysis of Structures* (Computers and Structures, Inc., 1995), pp. 1 and 19.
[22] Y.-H. Wu, Y.-H. Lin, H. Ren, X. Nie, J.-H. Lee, and S.-T. Wu, Opt. Express **13**, 4638 (2005).
[23] S. M. Clarke and E. M. Terentjev, Phys. Rev. Lett. **81**, 4436 (1998).